A Journal of the Gesellschaft Deutscher Chemiker

Angewandte International Edition GDCh Chemie

www.angewandte.org

Accepted Article

Title: Snapshots of a Migrating H-atom: Characterization of a Reactive Fe(III) Indenide Hydride and its Nearly Isoenergetic Ring-Protonated Fe(I) Isomer

Authors: Marcus Walter Drover, Dirk J. Schild, Paul H. Oyala, and Jonas Peters

To be cited as: *Angew. Chem. Int. Ed.* 10.1002/anie.201909050
Angew. Chem. 10.1002/ange.201909050

Link to VoR: http://dx.doi.org/10.1002/anie.201909050
http://dx.doi.org/10.1002/ange.201909050

WILEY-VCH

10.1002/anie.201909050

Accepted Article

Snapshots of a Migrating H-atom: Characterization of a Reactive Fe(III) Indenide Hydride and its Nearly Isoenergetic Ring-Protonated Fe(I) Isomer

Marcus W. Drover, Dirk J. Schild, Paul H. Oyala, and Jonas C. Peters*

Division of Chemistry and Chemical Engineering, California Institute of Technology, Pasadena, California, 91125, United States

Supporting Information Placeholder

ABSTRACT: We report the characterization of an S = ½ iron π-complex, [Fe(η^6-IndH)(depe)]$^+$ (Ind = Indenide ($C_9H_7^-$), depe = 1,2-*bis*(diethylphosphino)ethane), which results *via* C-H elimination from a transient Fe^{III} hydride, [Fe(η^3:η^2-Ind)(depe)H]$^+$. Owing to weak M-H/C-H bonds, these species undergo proton-coupled electron transfer (PCET) to release H_2 through bimolecular recombination. Mechanistic information, gained from stoichiometric as well as computational studies, reveal the open-shell π-arene complex to have a BDFE$_{C\text{-}H}$ value of ≈ 50 kcal mol^{-1}, roughly equal to the BDFE$_{Fe\text{-}H}$ of its Fe^{III}-H precursor (ΔG^o ≈ 0 between them). Markedly, this reactivity differs from related Fe(η^5-Cp/Cp*) compounds, for which terminal Fe^{III}-H cations are isolable and have been structurally characterized, highlighting the effect of a benzannulated ring (indene). Overall, this study provides a structural, thermochemical, and mechanistic foundation for the characterization of indenide/indene PCET precursors and outlines a valuable approach for the differentiation of a ring- versus a metal- bound H-atom by way of continuous-wave (CW) and pulse EPR (HYSCORE) spectroscopic measurements.

INTRODUCTION

For decades, cyclopentadienyl (Cp, $C_5H_5^-$) and derivatives thereof have been used as ligands to stabilize transition metal,[1] *f*-block,[2] and main-group[3] elements alike. This ligand class is ubiquitous among the synthetic community, no doubt a consequence of several alluring features, including variable hapticity,[4] whereby multiple coordination modes can be accommodated, ranging from η^1-to-η^5. There has been a surge of renewed interest in cooperative transformations with Cp-type ligands,[5] with protonation at such "non-innocent" rings being implicated in the context of hydride or proton-coupled-electron-transfer (PCET) pathways, for instance in H_2-evolving or dinitrogen reduction reactions (Chart 1A).[5,6]

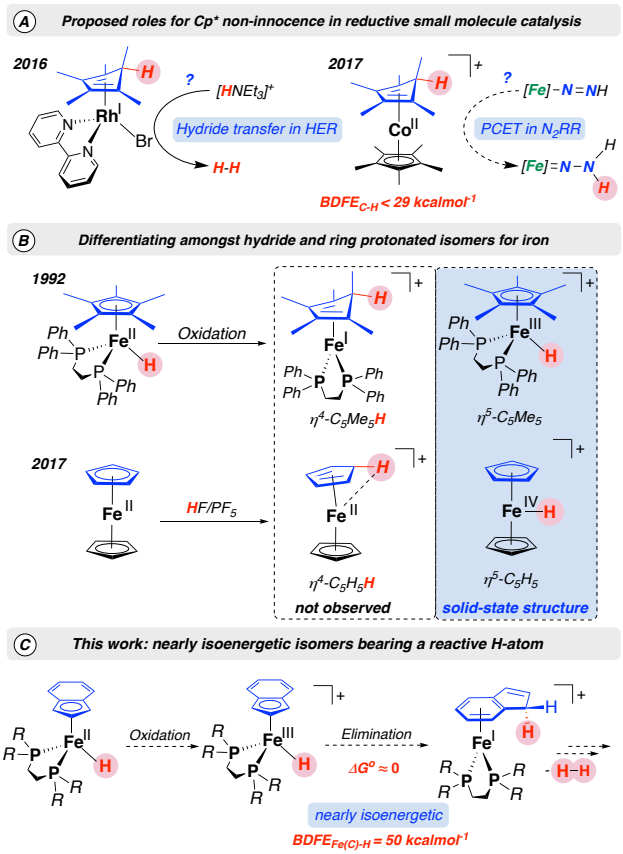

Chart 1. Previous work highlighting **A**) Cp* non-innocence for small-molecule fixation, **B**) interest in assigning H-atom location by XRD analysis, and **C**) the present study, featuring indene as a supporting ligand.

Metallocene ($Cp_2'M$) and half-sandwich complexes have been probed for decades in the context of ring protonation (or hydride attack) chemistry.[7] For species that are comparatively stable, characterization data for complexes wherein a ring is "protonated" can be distinguished from those wherein the "proton" instead resides on the metal as a hydride ligand. In certain cases, the H-atom may shuttle between these two positions. For example, the [Fe^{III}-H]$^+$ cation, [Fe^{III}(η^5-Cp*)(dppe)H]$^+$ (Cp* = $C_5Me_5^-$, dppe = 1,2-

bis(diphenylphosphino)ethane) is resistant to ring protonation (C-H elimination), but undergoes CO binding/reduction by $CoCp_2$ to give the diamagnetic complex $Fe^0(\eta^4\text{-}Cp^*H)(dppe)(CO)$ where H-migration has occurred onto the Cp*-ring.[8] More recently, crystallography has been used to show that protonation of ferrocene (Cp_2Fe) using a mixture of HF/PF_5 occurs at Fe, in spite of DFT calculations that favor (by 2 kcal mol^{-1}) a ring-protonated isomer, $CpFe(\eta^4\text{-}CpH)^+$ (Chart 1B).[7e] Distinguishing such species when the respective M-H or C-H bonded isomers feature weak and hence reactive bonds (low homolytic bond dissociation free energies: $BDFE_{M\text{-}H}$ and $BDFE_{C\text{-}H}$) is particularly challenging, especially for species that are open-shell. A recent study from our lab underscores this point, where protonation of Cp^*_2Co is thermodynamically favored at the ring (and not at Co); multi-frequency continuous-wave (CW) and pulse-EPR spectroscopies were performed at very low temperature to assign the site(s) of protonation.[6]

As part of an effort to extend such studies to other systems, our attention turned to iron hydride precursors of the type $Fe^{II}(\eta^3\text{:}\eta^2\text{-Ind})(P_2)H$ (Ind = indenide, $C_9H_7^-$, P_2 = diphosphine ligand), wherein an indenyl ligand was selected in an effort to stabilize reactive, ring-protonated complexes through [Fe]-η^6-IndH coordination, providing 6e$^-$ through the π-system (Chart 1C). To our surprise, for the system described herein, the isomer of the metal-bound hydride (formally Fe(III)) is nearly isoenergetic to the isomer in which the ring is instead protonated (formally Fe(I)). This represents, what is to our knowledge, an exceptional case. In general, only one of the isomers is experimentally observed.

Herein, we present the characterization of this pair of S = ½ Fe isomers, wherein H-atom migration has been validated in the solution state by CW- and pulse-EPR spectroscopy. For the Fe(I) indene complex, an X-ray crystal structure has been obtained. The data presented provide a means for facile differentiation between isomers of these types. Finally, a combination of experiment and theory provides access to relevant thermochemistry, including respective homolytic bond dissociation free energies:

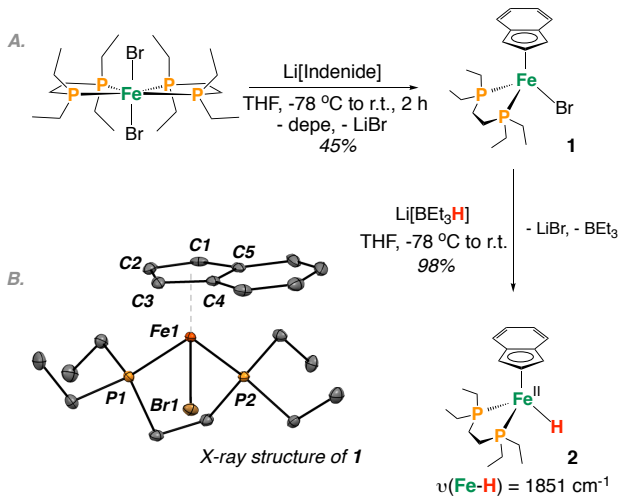

Figure 1. **A**) Synthesis of **2** by addition of $Li[BEt_3H]$. **B**) Solid-state structure of **1** with ellipsoids shown at 50% probability.

$BDFE_{C\text{-}H}$ and $BDFE_{Fe\text{-}H}$. Facile PCET from either an Fe-H or C-H bond is predicted to be feasible, and is exemplified by the propensity of the system to liberate H_2 in solution.

RESULTS AND DISCUSSION

Synthetic entry into the system of present interest is as follows: *trans*-$[Fe(Br)_2(depe)_2]$[9] (depe = 1,2-*bis*(diethylphosphino)ethane) was reacted with lithium indenide at −78 °C with warming to room-temperature over 2 h, providing $Fe(\eta^3\text{:}\eta^2\text{-Ind})(depe)Br$ (**1**) as a purple powder following work-up (δ_P = 92.98) (Figure 1A). Single crystals of **1** were grown from a saturated pentane-layered THF solution and analyzed by X-ray diffraction (XRD) at 100 K (Figure 1B). Consistent with $\eta^3\text{:}\eta^2$ binding, the structure features short Fe(1)-C(1)/C(2)/C(3) bond lengths (avg. = 2.078(2) Å) and long Fe(1)-C(4)/C(5) (avg. = 2.206(4) Å) contacts, with $\Delta(M\text{-}C)$[10] = 0.134 Å [Δ(M-C) = difference between these two averages] – this is true for all complexes discussed herein.

Complex **1** serves as a versatile starting material from

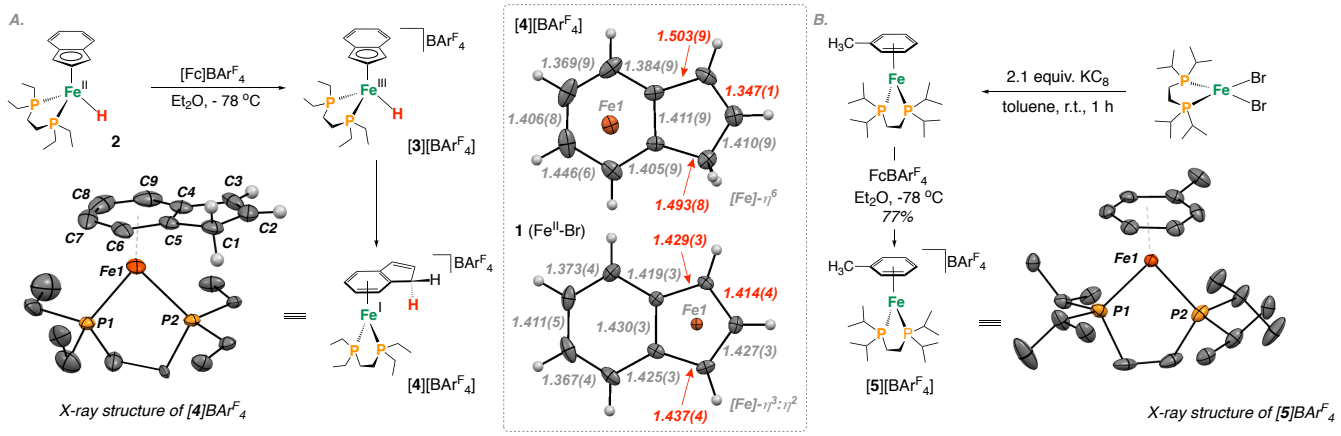

Figure 2. **A**) Synthesis of [**4**][BAr^F_4] by oxidation using [Fc]BAr^F_4 and solid-state depiction of the solid-state molecular structure of [**4**][BAr^F_4] with ellipsoids shown at 50% probability). Selected bond lengths [Å] and angles (°): Fe(1)-P(1) 2.222(3), Fe(1)-P(2) 2.298(3), Fe(1)-C(centroid), 1.589, ϕ([C(1)-C(5)]-[P(1)-Fe(1)-P(2)]), 90. **B**) Synthesis of [**5**][BAr^F_4] and solid-state depiction of the solid-state molecular structure of [**5**][BAr^F_4].

which the Fe^{II}-hydride, Fe(η^3:η^2-Ind)(depe)H (**2**) can be accessed (Figure 1A).[11] Reaction of **1** with Li[BEt$_3$H] gives **2** in near-quantitative yield. Most characteristically, the ^{31}P NMR spectrum provides a doublet at δ_P = 92.98 ppm ($^2J_{P,H}$ = 70.8 Hz, $^1J_{Fe,P}$ = 60.3 Hz: for **2**-^{57}Fe) that directly couples with the Fe^{II}-H group at δ_H = -20.64 ppm ($^1J_{Fe,H}$ = 10.7 Hz).

Complex **2** was also studied by cyclic voltammetry (CV), which reveals an irreversible feature centered at $E_{1/2}$ = - 0.81 V *vs.* Fc/Fc$^+$ (Fc = ferrocene) associated with the Fe^{II}/Fe^{III} couple; only ~75% of the signal current is maintained on the return reductive wave (*SR* = 50 mV/s), suggesting reactivity of the *in-situ* generated Fe(III) cation.[12] Given our desire to generate a reactive open-shell [Fe(III)-H]$^+$ species, we next probed the oxidative chemistry of complex **2** using [Fc]BAr$^F_4$ ($E_{1/2}$ = 0 V *vs.* Fc/Fc$^+$; Ar$^F_4$ = 3,5-(CF$_3$)$_2$(C$_6$H$_3$)),[13] at −78 °C (Figure 2).

Monitoring this reaction mixture for both ^{1}H and ^{2}H isotopologues by freeze-quenched X-band CW-EPR spectroscopy (77 K) shows the formation of a single S = ½ species exhibiting roughly axial symmetry (g = [2.377, 2.039, 1.993]) with couplings of similar magnitude to two distinct ^{31}P (I = 1/2) nuclei. Significant additional couplings to ^{1}H are resolved in the ^{1}H isotopologue, consistent with the presence of a strongly coupled hydride ^{1}H nucleus (Figure 3A): thus we assign this spectrum to [Fe^{III}(η^3:η^2-Ind)(depe)H][BAr$^F_4$] [**3**]$^+$. Collection of a series of X-band Davies ENDOR spectra across the EPR envelope of [**3**-D]$^+$ (*see ESI*) provide additional data showing large coupling to two non-equivalent phosphines (A(^{31}Pα) = ± [100, 88, 88] MHz and A(^{31}Pβ) = ± [82, 85, 72] MHz).

To determine more accurate hyperfine parameters for the hydride ligand than can be resolved from CW-EPR, we turned to X-band ^{2}H-HYSCORE of this same [**3**-D]$^+$ isotopologue. Simulation of field-dependent HYSCORE spectra of [**3**-D]$^+$ reveal a highly anisotropic deuterium hyperfine tensor A(^{2}H) = ± [1.84, 12.6, 10.0] MHz, with a

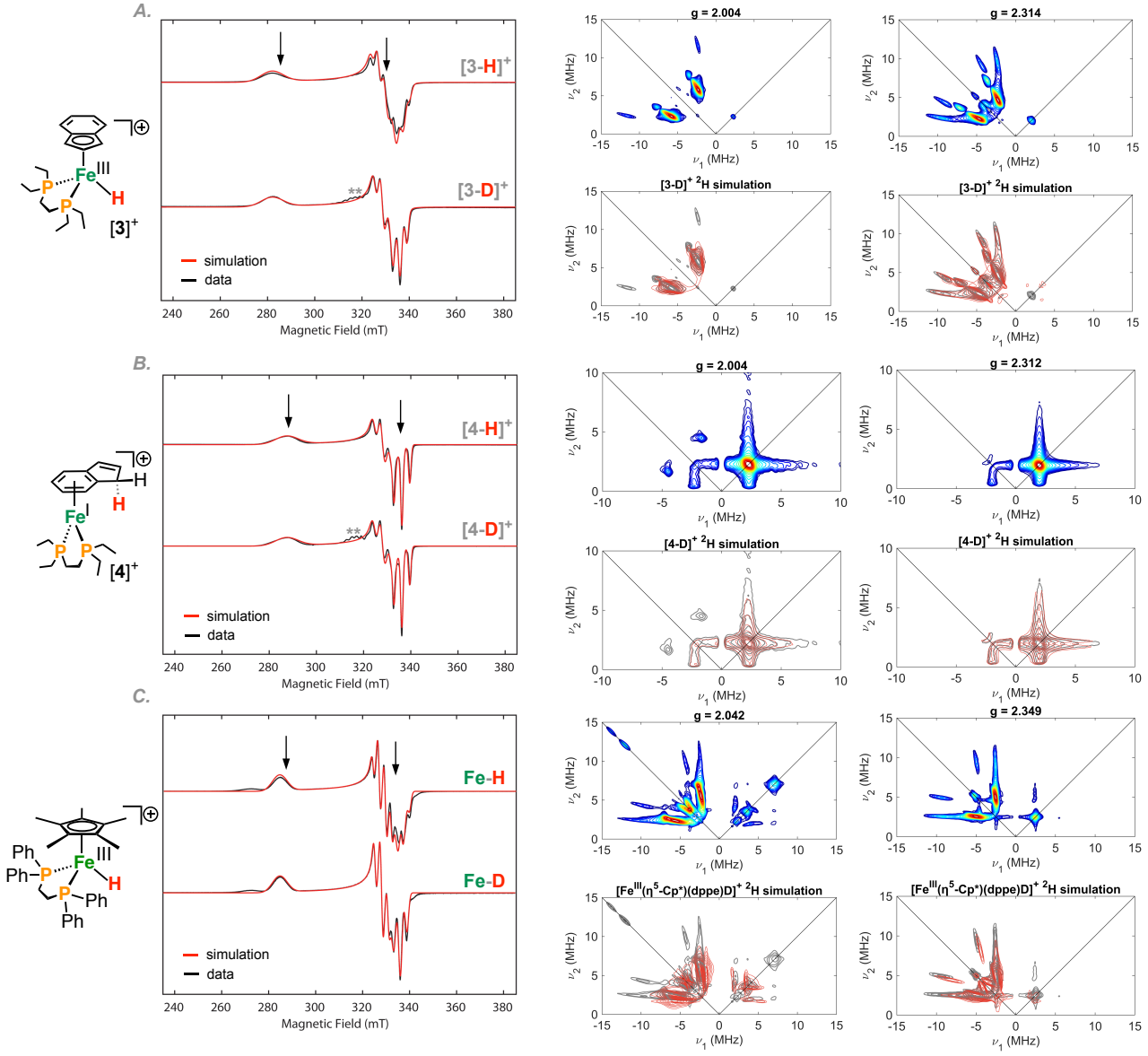

Figure 3. Freeze-quenched X-Band EPR spectrum (9.371 GHz) and corresponding X-band HYSCORE data recorded in 2-MeTHF glass at 77 K. **A**) [**3-H**][BAr$^F_4$] and [**3-D**]BAr$^F_4$; **B**) [**4-H**]BAr$^F_4$ and [**4-D**]BAr$^F_4$ and **C**) [Fe^{III}(η^5-Cp*)(dppe)H]$^+$ and [Fe^{III}(η^5-Cp*)(dppe)D]$^+$ HYSCORE simulations of the ^{2}H hyperfine couplings are overlaid in red over the data, which is plotted in grey. Downward pointed arrows represent g-values at which HYSCORE has been acquired. ** = [Fe(depe)$_2$(N$_2$)]BAr$^F_4$[18] impurity.

10.1002/anie.201909050

small Euler rotation of the hyperfine tensor relative to the g-tensor of (α,β,γ) = (40, 15, 0)°. Scaling of the ^{2}H hyperfine tensor determined by ^{2}H HYSCORE by the proportion of ^{1}H/^{2}H gyromagnetic ratios (γ^1H/γ^2H = 6. 514) provides a ^{1}H hyperfine tensor $A(^1\text{H})$ = ± [12, 82, 65] MHz which is in agreement with simulation of the X-band CW-EPR spectrum. This hyperfine coupling tensor consists of both large isotropic ($a_{iso}(^1\text{H})$ = ± 53 MHz) and anisotropic ($T(^1\text{H})$ = ± [-41, 29, 12] MHz) components, consistent with those expected for a terminal metal hydride.[14]

For comparison, we have also undertaken study of Lapinte's *bonafide* S = ½ Fe^{III}-H species (for which an X-ray structure is available),[11a] Fe^{III}(η^5-Cp*)(dppe)H$^+$. Analogous EPR characterization reveals spectroscopic features consistent with those discussed above, namely, a large and very anisotropic ^{1}H coupling of $A(^1\text{H})$ = ± [4, 68, 50] MHz ($a_{iso}(^1\text{H})$ = ± 40.7 MHz, $T(^1\text{H})$ = ± [-36.7, 27.3, 9.3] MHz) (Figure 6).

Although at early reaction periods an Fe^{III}-H species is observed, timed freeze-quench experiments show this complex is consumed at −78 °C ($t_{1/2}$ = 15 min) to provide a new roughly axial S = ½ species with g = [2.332, 2.042, 1.992].[15] X-band ENDOR spectroscopy provides data (*see ESI*) that is consistent with large coupling to two non-equivalent phosphines ($A(^{31}\text{P}\alpha)$ = ± [86, 104, 100] MHz and $A(^{31}\text{P}\beta)$ = ± [93, 88, 94] MHz). Unlike in the case of the terminal hydride species, Fe^{III}-H/D [**3**]$^+$ and [**3-D**]$^+$, no difference in the CW X-band EPR spectrum between [**4**]$^+$ and [**4-D**]$^+$ (associated with a large anisotropic ^{1}H coupling) is noted. Further analysis by ^{1}H/^{2}D difference HYSCORE spectroscopy reveals a very small anisotropic coupling to a single ^{1}H nucleus, $A(^1\text{H})$ = ± [1, -4, -4] MHz, which we assign to an indene ring proton, formed by C-H elimination to give [Fe^I(η^6-IndH)(depe)]$^+$ ([**4**]$^+$). Consistent with the DFT-calculated spin-density plot for [**4**]$^+$, the Fe-bound indene fragment is observed to bear minimal spin *c.f.* the terminal hydide [**3**]$^+$ (Figure 4). Calculated and experimental EPR parameters are summarized in Figure 6.

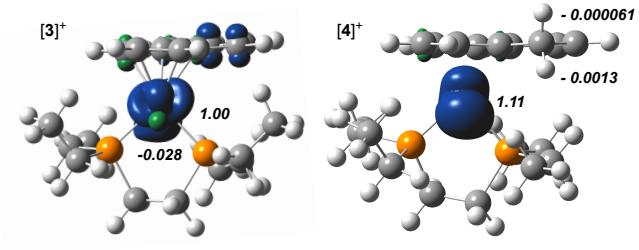

Figure 4. DFT-calculated spin-density plot for [**3**]$^+$ and [**4**]$^+$ (isovalue: 0.004 *e*-/Å^3; TPSS; def2tzvp (Fe), def2svp (all other atoms).

To ensure appropriate assignment of complex [**4**]$^+$ by EPR spectroscopy, the S = ½ model compound, [Fe(η^6-toluene)(dippe)][BAr$^F_4$] ([**5**]$^+$) (dippe = 1,2-*bis*(diisopropylphosphino)ethane) was prepared by oxidation of Fe(η^6-toluene)(dippe)[16] with [Fc]BAr$^F_4$ at -78 °C (Figure 2). By EPR spectroscopy, a similar spectrum to that of [**4**]$^+$ was acquired, with simulation parameters appropriate for a rhombic species with g = [2.371, 2.032, 1.990 (Figure 5).

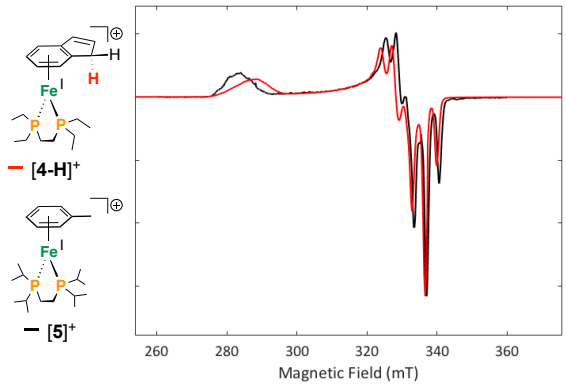

Figure 5. Freeze-quenched X-Band EPR spectrum (9.386 GHz) recorded in 2-MeTHF glass at 77 K for [**4-H**]BAr$^F_4$ (red) and [**5**]BAr$^F_4$ (black).

Despite its propensity to lose H_2 (vide infra), the assignment of [**4**]$^+$ could be further cemented by storing one such oxidation mixture cold, providing orange blocks suitable for XRD analysis (Figure 2A). On first inspection, the Fe-P contacts for this open-shell d^7 system were noted to be longer than those for the S = 0 variant (complex **1**, for example) with values of 2.222(3)/2.298(3) Å compared to 2.1792(6)/2.2217(6) Å. Furthermore, metrics associated with the dearomatized five-membered indene ring are markedly different, with elongation along the C(1)-C(5) and C(3)-C(4) vectors [1.437(4)/1.429(3) Å to 1.493(8)/1.503(9) Å] and contraction along the C(2)-C(3) vector [1.414(4) to 1.347(1) Å], signifying new single and double bonds, respectively.[17] The presence of a "two-legged piano stool" complex is further corroborated by ϕ, where the plane created by P(1)-Fe(1)-P(2) is perfectly perpendicular (90°) to the iron-bound indene ring. For complex [**5**]$^+$, similar data were also obtained providing Fe-P contacts [2.2272(2)/2.254(2) Å] and a ϕ value [96.7°] close to that of [**4**]$^+$ [2.222(3)/2.298(3) Å and ϕ = 90°] (Figure 2B).

10.1002/anie.201909050

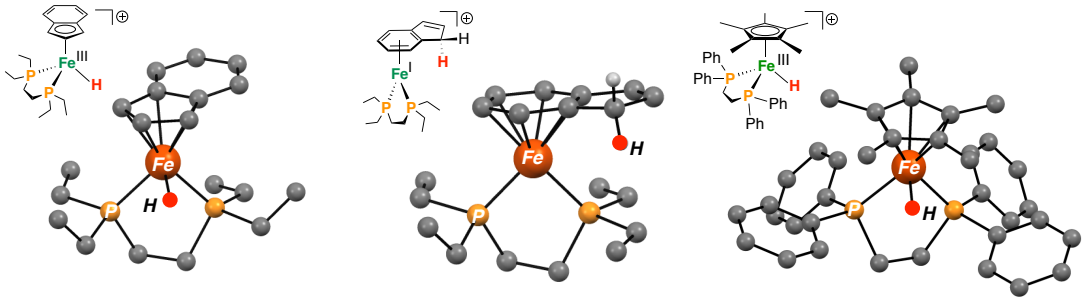

	[Fe^{III}(η^5-Ind)(depe)(H)]$^+$ ([3]$^+$)	[Fe^{I}(η^6-IndH)(depe)]$^+$ ([4]$^+$)	[Fe^{III}(η^5-Cp*)(dppe)(H)]$^+$
	G = 0 kcal mol^{-1} $BDFE_{Fe\text{-}H}$ = 50 kcal mol^{-1}	G_{rel} = 0 kcal mol^{-1} $BDFE_{C\text{-}H}$ = 50 kcal mol^{-1}	— $BDFE_{Fe\text{-}H}$ = 56 kcal mol^{-1}
	g = [2.377, 2.039, 1.993]	g = [2.332, 2.042, 1.992]	g = [2.352, 2.041, 1.992]
	$A(^{31}P_\alpha)$ = ± [100, 88, 88] MHz $A(^{31}P_\beta)$ = ± [82, 85, 72] MHz	$A(^{31}P_\alpha)$ = ± [86, 104, 100] MHz $A(^{31}P_\beta)$ = ± [93, 88, 94] MHz	$A(^{31}P_\alpha)$ = ± [88, 82, 79] MHz $A(^{31}P_\beta)$ = ± [82, 71, 76] MHz
	$A(^1H)$ = ± [12, 82, 65] MHz $a_{iso}(^1H)$ = ± 53 MHz $T(^1H)$ = ± [-41, 29, 12] MHz	$A(^1H)$ = ± [-1, -4, -4] MHz $a_{iso}(^1H)$ = ± 2.3 MHz $T(^1H)$ = ± [3.3, -1.7, -1.7] MHz	$A(^1H)$ = ± [4, 68, 50] MHz $a_{iso}(^1H)$ = ± 40.7 MHz $T(^1H)$ = ± [-36.7, 27.3, 9,3] MHz
DFT	$A(^1H)$ = [-15.4, -74.8, -73.2] MHz $a_{iso}(^1H)$ = -54.5 MHz $T(^1H)$ = [39.1, -20.3, -18.7] MHz	$A(^1H)$ = [1.1, -4.2, -4.6] MHz $a_{iso}(^1H)$ = -2.6 MHz $T(^1H)$ = [3.6, -1.7, -2] MHz	$A(^1H)$ = [-1.2, -59.9, -58.0] MHz $a_{iso}(^1H)$ = -39.7 MHz $T(^1H)$ = [38.5, -20.2, -18.3] MHz

Figure 6. DFT optimized structures of [**3**]$^+$, [**4**]$^+$, and [Fe^{III}(η^5-Cp*)(dppe)H]$^+$. Experimental and theoretical A(^{1}H) values are shown for the proton coded with a red circle. Equations: a_{iso} = [A_x + A_y + A_z]/3, T(^{1}H) = [A_x - a_{iso}, A_y - a_{iso}, A_z - a_{iso}]. DFT: Structures were optimized using TPSS; def2tzvp (Fe), def2svp (all other atoms) and EPR calculations: CP(PPP) (Fe), TPSS/IGLO-III (all other atoms).

Complexes [**3**]$^+$ and [**4**]$^+$ undergo bimolecular degradation in solution, resulting in H_2 loss (Figure 7). For example, reaction of **2** with [Fc]BAr$^F{}_4$ in Et_2O at −78 °C and warming to room-temperature results in visible precipitation of a maroon solid and formation of H_2 (~60% H_2 as quantified by GC). Analysis of the crude ^{31}P NMR spectrum (THF-d_8) evidences two major by-products that are assignable to [Fe(η^3:η^2-Ind)(depe)N_2][BAr$^F{}_4$] ([**6**]$^+$; υ_{NN} = 2151 cm^{-1}, *ca.* 20%) and [Fe$_2$(η^3:η^2-Ind)$_2$(depe)$_2$(μ-depe)][BAr$^F{}_4$]$_2$ ([**7**]$^{2+}$; *ca.* 20%), respectively.[18] Consistent with formation of these two species, cooling of the reaction mixture produces yellow and violet crystals suitable for analysis by XRD (Figure 7B). Presumably these compounds are formed from bimolecular H_2 release from one (or more) of the following pairs: {[Fe^{III}]–H···H–[Fe^{III}]}‡, {[Ind]C–H···H–[Fe^{III}]}‡, or {[Ind]C–H···H–C[Ind]}‡.[19] To confirm bimolecular H_2 release, a 1:1 ratio of **2-H** and **2-D** was mixed, followed by oxidation with [Fc]BAr^F at −78 °C, and allowing the solution to warm. The release of HD, as detected by NMR spectroscopy, substantiates a bimolecular H-H coupling process.

To experimentally benchmark the H• transfer propensity of [**4**]$^+$, we aimed to determine an upper limit for $BDFE_{Fe\text{-}H}$ which, based on the small energy difference between [**3**]$^+$ and [**4**]$^+$ (*vide infra*), should be similar to $BDFE_{C\text{-}H}$. Figures 8A-C summarizes our findings via experiment and theory. Reaction of an MeCN solution of **2** with 1-benzyl-3-acetylpyridinium [BNAP]OTf[20] results in hydride transfer and clean formation of [Fe(η^3:η^2-Ind)(depe)(NCCH$_3$)]$^+$ [**8**]$^+$ (δ_P = 92.8 ppm) (Figure 8). Transfer also proceeds in THF, providing the N_2-adduct, [**6**]$^+$ and μ-depe complex, [**7**]$^{2+}$. The hydricity (defined as the heterolytic dissociation energy of M–H to give M$^+$ and H$^-$ (ΔG(**2**)$_{H^-}$) of **2** in MeCN must therefore be less than the hydricity of 1,4-BNAPH (ΔG_{H^-} ≈ 60 kcal mol^{-1}), *i.e.* more

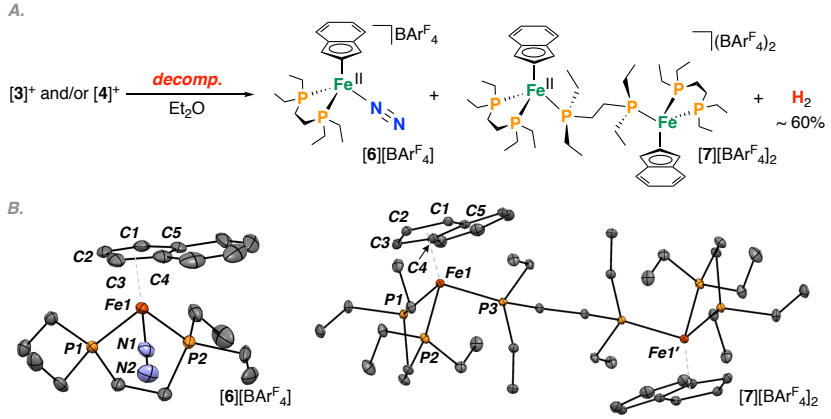

Figure 7. **A**) Decomposition of [**3**]$^+$ and [**4**]$^+$. **B**) Solid-state depiction of [**6**][BAr$^F{}_4$] and [**7**][BAr$^F{}_4$]$_2$. (displacement ellipsoids are shown at the 50% probability). Selected bond length for [**6**][BAr$^F{}_4$]: N(1)-N(2)) = 1.108(6) Å.

hydridic.[21] In theory, loss of H^- from **2** should give [Fe(η^3:η^2-Ind)(depe)]$^+$, though this cation is not observed experimentally due to facile MeCN binding to give the adduct (ΔG^o(DFT) = - 17 kcal mol^{-1}; Fig. 8C). For comparison, hydricities of 54 kcal mol^{-1} and an upper bound of < 44 kcal mol^{-1} have been established for the six-coordinate terminal iron hydrides, $(SiP_3)Fe(H)(H_2)$[22] and $(SiP_2S)Fe(H)(H_2)$[14b], respectively.

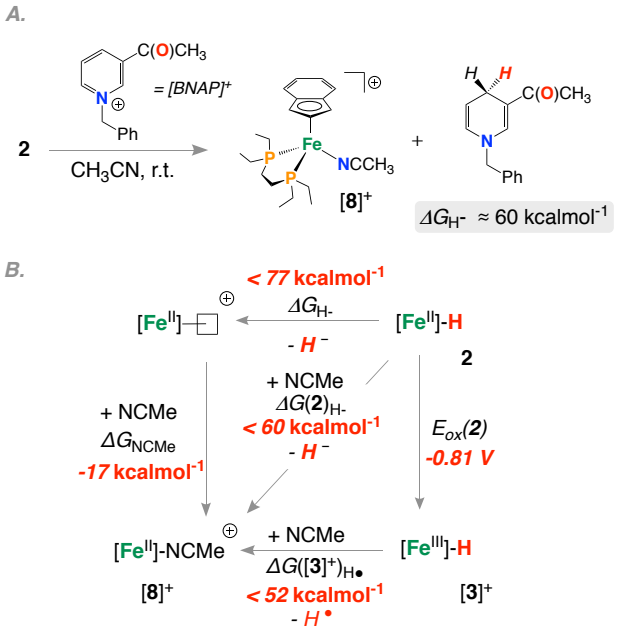

Figure 8. **A**) Reaction of **2** with 1-benzyl-3-acetylpyridinium triflate (BNAP)$^+$; **B**) Square scheme for experimentally calculated thermodynamic quantities. **C)** Thermodynamic relationships that relate H$^•$ and H$^-$ transfer in MeCN.

Utilizing thermodynamic relationships that relate H$^•$ and H$^-$ in MeCN,[23] the upper bound for the free energy of H$^-$ transfer from **2** and H$^•$ transfer from [**3**]$^+$ can be related (eqns. 4 and 5, Figure 8C). The [Fe]–H bond of [**3**]$^+$ is thus conservatively estimated to have an upper bound BDFE ($\Delta G([\mathbf{3}]^+)_{H•}$) of < 52 kcal mol^{-1} giving [Fe(η^3:η^2-Ind)(depe)(NCCH$_3$)]$^+$ and H$^•$; the DFT-predicted value is 33 kcal mol^{-1} (TPSS; def2tzvp (Fe), def2svp (all other atoms)) – these values suggest that, on the basis of thermodynamics alone, loss of H_2 should be facile ($BDFE_{H\text{-}H}$ = 102.3 kcal mol^{-1} in CH_3CN).[24]

To gain insight into the elementary steps associated with the reactivity of these species, we turned to DFT (Figure 9). First, a negligible energy difference is calculated between [**3**]$^+$ (**I**) and [**4**]$^+$ (**II**) ($\Delta G^o \approx 0$ kcal mol^{-1}), which we attribute to stabilization of [**4**]$^+$ by η^6-indene coordination. For a related family of compounds, $Fe^{III}(\eta^5\text{-}C_5R_5)(P_2)H^+$ (R = H, P_2 = dippe (1,2-bis(diisopropylphosphino)ethane or R = CH_3, P_2 = dppe),[11] hydride-to-ring migration is not observed. In this regard, a difference of + 13 kcal mol^{-1} is calculated between the theoretical compounds, [Fe^I(η^4-CpH)(depe)]$^+$ and [Fe^{III}(η^5-Cp)(depe)H]$^+$, and an even larger value of + 16 kcal mol^{-1} is calculated between [Fe^I(η^4-Cp*H)(depe)]$^+$ and [Fe^{III}(η^5-Cp*)(depe)H]$^+$, (Figure 10). These values do not correlate with the higher basicity of Cp*H (pKa = 26.1) versus IndH (pKa = 20.1) versus CpH (pKa = 18.0) and are instead likely ascribable to ligand steric effects.[25] Nonetheless, for this family of complexes, only the indene system manifests ring functionalization by H-migration due to a 9 kcal mol^{-1} stabilization resulting from ring slippage.

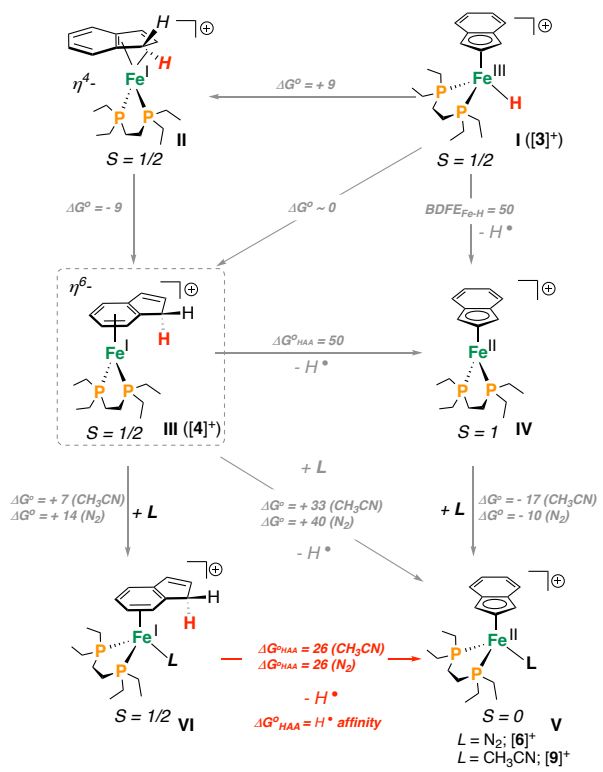

Figure 9. Free energy change (kcal mol^{-1}) for PCET involving $BDFE_{C\text{-}H}$ (TPSS; def2tzvp (Fe), def2svp (all other atoms)).

In terms of $BDFE_{C\text{-}H}$, the 17-electron complex **III** is calculated to have a $BDFE_{C\text{-}H}$ of 50 kcal mol^{-1}, and the terminal hydride **I** is calculated to possess an equivalent energy ($BDFE_{Fe\text{-}H}$ = 50 kcal mol^{-1}); both pathways provide the vacant S = 1 cation, [Fe(η^3:η^2-Ind)(depe)]$^+$ (**IV**) and H$^•$, indicating that both species should be competent for H_2 loss.[22] By contrast, we calculate [Fe^{III}(η^5-Cp*)(dppe)H]$^+$ to possess a stronger Fe-H bond: $BDFE_{Fe\text{-}H}$ = 56 kcal mol^{-1}. We find experimentally this Fe^{III}-H cation is stable in ethereal solvent (by UV-VIS and ^{1}H NMR spectroscopy) and does not release H_2 under ambient conditions (< 5% decomposition after 1 week).

Alternatively, from the 17-electron cation **III**, 19-electron complexes **VI** can be optimized upon associative substitution of a two-electron donor (L) with the hydrogen atom affinity ΔG^o_{HAA} being 26 kcal mol^{-1} for both L = $NCCH_3$ and N_2. In this transformation, the driving force for **III** → **V** is proposed to be a dual consequence of i) in-

10.1002/anie.201909050

dene rearomization and ii) formation of a stable 18-electron product.

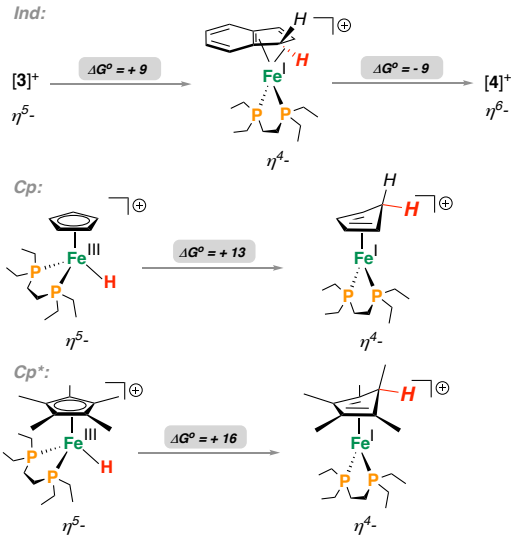

Figure 10. DFT-predicted free energy change (kcal mol^{-1}) for metal-to-ring H-migrations.

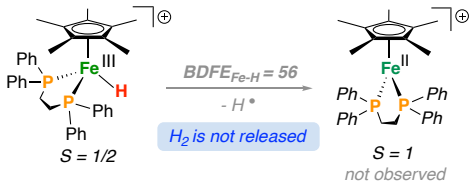

Figure 11. Free energy change (kcalmol^{-1}) for PCET using [Fe^{III}(η^5-Cp*)(dppe)H]$^+$ (TPSS; def2tzvp (Fe), def2svp (all other atoms)).

CONCLUSION

We have described the synthesis, electronic characterization, and thermochemistry associated with a pair of isomeric open-shell S = ½ complexes, [Fe^{III}(η^2:η^3-Ind)(depe)H]$^+$ and [Fe^{I}(η^6-IndH)(depe)]$^+$. By calculation and experiment, we have shown that these species are highly reactive, having C-H and Fe-H bonds that are close in energy (BDFE$_{C\text{-}H}$ ≈ BDFE$_{Fe\text{-}H}$ ≈ 50 kcal mol^{-1}) manifesting in PCET to provide H$^\bullet$ (identified as H_2), presumably through bimolecular combination of one (or more) of the following pairs: {[Fe^{III}]–H···H–[Fe^{III}]}‡, {[Ind]C–H···H–[Fe^{III}]}‡, or {[Ind]C–H···H–C[Ind]}‡. With a unique opportunity to observe both species, detailed X-band (CW) and pulse EPR spectroscopic experiments were undertaken, that together, provide a reliable means to differentiate a ring- versus a metal- bound H-atom – an approach that should prove useful in other systems for which ligands might play a non-innocent role in hydride, proton, or hydrogen atom transfer. Ongoing studies in our laboratory are currently focused on exploiting the PCET reactivity of weak C-H bonds in this and related systems.

ASSOCIATED CONTENT

Supporting Information

^{1}H, ^{13}C{^{1}H}, and ^{31}P{^{1}H} NMR spectra for complexes, ^{57}Mössbauer, UV-Vis, IR, and EPR spectroscopy as well as crystallographic data for **1**, **4**, [**5**][BAr$^F_4$], [**6**][BAr$^F_4$], and [**7**][BAr$^F_4$]$_2$. CCDC **1896047-1896051** contains the supplementary crystallographic data for this paper. These data can be obtained free of charge from The Cambridge Crystallographic Data Centre *via* www.ccdc.cam.ac.uk/data_request/cif.

AUTHOR INFORMATION

Corresponding Author

*jpeters@caltech.edu

Notes

The authors declare no competing financial interest.

ACKNOWLEDGEMENTS

The authors are grateful to the Department of Energy for support *via* Grant No. DOE-0235032. The Caltech EPR facility was supported by the National Science Foundation *via* grant No. NSF MRI-153194, as well as the Dow Next Generation Educator Fund. The Beckman Institute is thanked for X-ray support. M.W.D. acknowledges NSERC (Banting PDF award to MWD), and M.W.D. / D. J. S thank the Resnick Sustainability Institute at Caltech for fellowships.

REFERENCES

[1] a) Collman, J. P.; Hegedus, L. S.; Norton, J. R.; Finke, R. G. Principles and Applications of Organotransition Metal Chemistry. University Science Books, CA, **1987**; b) Crabtree, R. H. The Organometallic Chemistry of the Transition Metals, 2nd ed., John Wiley & Sons, NY, **1994**.

[2] Poli, R. *Chem. Rev.* **1991**, *91*, 509; b) Evans, W. J. *Organometallics* **2016**, *35*, 3088.

[3] a) Jutzi, P.; Reumann, G. *J. Chem. Soc. Dalton Trans.* **2000**, *14*, 2237; b) Budzelaar, P. H.; Engelberts, J. J.; van Lenthe, J. H. *Organometallics* **2003**, *22*, 1562.

[4] a) Gridnev, I. D. *Coord. Chem. Rev.* **2008**, *252*, 1798; b) Veiros, L. F. *Organometallics* **2000**, *19*, 5549; c) O'Connor, J. M.; Casey, C. P. *Chem. Rev.* **1987**, *87*, 307.

[5] a) Quintana, L. M. A.; Johnson, S. I.; Corona, S. L.; Villatoro, W.; Goddard, W. A.; Takase, M. K.; VanderVelde, D. G.; Winkler, J. R.; Gray, H. B.; Blakemore, J. D. *PNAS* **2016**, *113*, 6409; b) Zamorano, A.; Rendón, N.; Valpuesta, J. E. V.; Álvarez, E.; Carmona, E. *Inorg. Chem.* **2015**, *54*, 6573; c) Pal, S.; Kusumoto, S.; Nozaki, K. *Organometallics* **2018**, *37*, 906; d) Moreno, J. J.; Espada, M. F.; Campos, J.; Lopez-Serrao, J.; Macgregor, S. A.; Carmona, E. *J. Am. Chem. Soc.* **2019**, *141*, 2205; e) Sapsford, J. S.; Gates, S. J.; Doyle, L. R.; Taylor, R. A.; Diez-Gonzalez, S.; Ashley, A. E. *Inorg. Chim. Acta.* **2019**, *488*, 201; f) Pitman, C. L.; Finster, O. N. L.; Miller, A. J. M. *Chem. Commun.* **2016**, *52*, 9105.

[6] Chalkley, M.; Del Castillo, T.; Matson, B.; Roddy, J.; Peters, J. C. *ACS Cent. Sci.* **2017**, *3*, 217; b) Chalkley, M. J.; Del

Castillo, T. J.; Matson, B.; Peters, J. C. *J. Am. Chem. Soc.* **2018**, *140*, 6122; c) Chalkley, M. J.; Oyala, P. H.; Peters, J. C. *J. Am. Chem. Soc.* **2019**, *141*, 4721-4729.

[7] a) Curphey, T. J.; Santer, J. O.; Rosenblum, M.; Richards, J. H. *J. Am. Chem. Soc.* **1960**, *82*, 5249−5250; b) Liles, D. C.; Shaver, A.; Singleton, E.; Wiege, M. B. *J. Organomet. Chem.* **1985**, *288*, c33−c36; c) Court, T. L.; Werner, H. *J. Organomet. Chem.* **1974**, *65*, 245−251; d) Koelle, U.; Khouzami, F. *Angew. Chem., Int. Ed. Engl.* **1980**, *19*, 640−641; e) Malischewski, M.; Seppelt, K.; Sutter, J.; Heinemann, F. W.; Birger, D.; Meyer, K. *Angew. Chem. Int. Ed.* **2017**, *56*, 13372.

[8] Hamon, P.; Hamon, J. R.; Lapinte, C. *J. Chem. Soc. Chem. Commun.* **1992**, 1602.

[9] Mays, M. J.; Prater, B. E. *Inorg. Synth.* **1974**, *15*, 21.

[10] Faller, J. W.; Crabtree, R. H.; Habib, A. *Organometallics* **1985**, *4*, 929.

[11] For related Fe(η^5-Cp)(P_2)H-derivatives, see: a) Hamon, P.; Toupet, L.; Hamon, J.R.; Lapinte, C. *Organometallics* **1992**, *11*, 1429; b) de la Jara Leal, A.; Tenorio, M. J.; Puerta, M. C.; Valerga, P. *Organometallics* **1995**, *14*, 3839.

[12] At greater scan rate (SR), reversibility increases.

[13] Connelly, N. G.; Geiger, W. E. *Chem. Rev.* **1996**, 96, 877-910.

[14] For example: a) Chiang, K. P.; Scarborough, C. C.; Horitani, M.; Lees, N. S.; Ding, K.; Dugan, T. R.; Brennessel, W. W.; Bill, E.; Hoffman, B. M.; Holland, P. L. *Angew. Chem., Int. Ed.* **2012**, *51*, 3658; b) Gu, N. X.; Oyala, P. H.; Peters, J. C. *J. Am. Chem. Soc.* **2018**, *140*, 6374.

[15] Monitoring the decay of [**3**]$^+$ at – 60 °C by UV/vis spectroscopy shows clean, first order kinetics (see ESI).

[16] Hermes, A. R.; Warren. T. H.; Girolami, G. S. *J. Chem. Soc. Dalton Trans.* **1995**, 301.

[17] Similar metrics are observed for other η^6-IndH (C_9H_8) complexes, see: a) Bercaw, J. E.; Hazari, N.; Labinger, J. A. *Organometallics* **2009**, 28, 5489; b) Fessenbecker, A.; Stephan, M.; Grimes, R. N.; Pritzkow, H.; Zenneck, U.; Siebert, W. *J. Am. Chem. Soc.* **1991**, *113*, 3061; c) Hung, M. Y.; Ng, M. S.; Zhou, Z.; Lau, C. P. *Organometallics* **2000**, *19*, 3692.

[18] Other side products were also identified including $Fe(depe)_2N_2^+$. This compound was analyzed by HYSCORE spectroscopy (see *ESI*), showing identical ^{14}N couplings to those determined by: Doyle, L. R.; Scott, D. J.; Hill, P. J.; Fraser, D. A. X.; Myers, W. K.; White, A. J. P.; Green, J. C.; Ashley, A. E. *Chem. Sci.* **2018**, *9*, 7362.

[19] See: a) Wayland, B. B.; Ba, S.; Sherry, A. E. *J. Am. Chem. Soc.* **1991**, *113*, 5305; b) Nocton, G.; Booth, C. H.; Maron, L.; Andersen, R. A. *Organometallics* **2013**, *32*, 1150; c) Halpern, J.; Pribanic, M. *Inorg. Chem.* **1970**, *9*, 2616.

[20] a) Zhang, F.; Jia, J.; Dong, S.; Wang, W.; Tung, C. -H. *Organometallics* **2016**, *35*, 1151; b) Zhang, F.; Xu, X.; Zhao, Y.; Jia, J.; Tung, C.- H. Wang, W. *Organometallics* **2017**, *36*, 1238.

[21] a) Ilic, S.; Kadel, U. P.; Basdogan, Y.; Keith, J. A.; Glusac, K. D. *J. Am. Chem. Soc.* **2018**, *140*, 4569; b) Ellis, W. W.; Raebiger, J. W.; Calvin, C. J.; Bruno, J. W.; DuBois, D. L. *J. Am. Chem. Soc.* **2004**, 126, 2738.

[22] Fong, H.; Peters, J. C. *Inorg. Chem.* **2015**, 54, 5124.

[23] a) Wiedner, E. S.; Chambers, M. B.; Pitman, C. L.; Bullock, R.M.; Miller, A. J. M.; Appel, A. M. *Chem. Rev.* **2016**, 116, 8655; b) Pearson, R. G. *Chem. Rev.* **1985**, *85*, 41.

[24] Warren, J. J.; Tronic, T. A.; Mayer, J. M. *Chem. Rev.* **2010**, *110*, 6961.

[25] Bordwell, F. G.; Bausch, M. J. *J. Am. Chem. Soc.* **1983**, *105*, 6188.